

## Thermal non-destructive testing: Modeling, simulation and experiments for improved localization of hidden defects

by S. Hatefipour<sup>1,3</sup>, J. Ahlberg<sup>2,3</sup>, J. Wren<sup>1,2</sup> and A. Runnemalm<sup>1</sup>

<sup>1</sup> University West, SE-461 86 Trollhättan, Sweden, {saeid.hatefipour, anna.runnemalm, joakim.wren}@hv.se

<sup>2</sup> Linköping University, SE-581 11 Linköping, Sweden, {jorgen.ahlberg, joakim.wren}@liu.se

<sup>3</sup> Termisk Systemteknik AB, Diskettgatan 11B, SE-583 35 Linköping, Sweden, {saeid, jorgen}@termisk.se

### Abstract

During the last decades, a substantial amount of research and practical work has been conducted on non-destructive testing of materials using thermography. The performed studies elucidate the potential of various types of thermal non-destructive testing (TNDT) for different materials and applications, including various types of defects. This paper presents a method for detecting in-depth defects in metallic materials and a simulation model for the heat transfer in the material. Experiments are performed on a test specimen with artificial defects (flat-bottom holes). The detection method exploits spatiotemporal analysis in order to find deviations from a model of normality, and shows novel results. Thermal modelling is performed in order to have a base-line simulation model enable us to (a) investigate affecting parameters without repeating the experiments and (b) generalize the results and extend their validity to other cases. Results show that there is an acceptable compliance between simulated and measured thermal data.

### 1. Introduction

Defect-free materials have become a vital issue for the aerospace and automotive industries. Various quality control methods have been developed and implemented so far, however, real time quality control using thermal non-destructive testing (TNDT) presents fast, contact-free, and proactive solutions for inspection of materials and components. The effect of applying thermal energy using various sources of heat stimulation for various materials and applications is investigated in [1-3]. Each of these methods has advantages for specific tasks. Several methods address the challenge of getting a higher image quality; therefore image processing/analysis have become a central issue within almost all thermal non-destructive testing (TNDT) problems [4-8].

In order to detect and characterize defects, TNDT in combination with image processing techniques for feature extraction and image enhancement is studied in [4-8]. In contrast, other publications [9-11] focus on detection and localization of defects by numerical modelling and simulation using e.g. the finite element method (FEM) in combination with experiments. Such studies facilitate not only defect detection and localization, but also investigations of the importance of influencing parameters in a more cost effective way compared with stand-alone experiments. Therefore, thermographic measurements, modeling and simulation in combination with image analysis approaches of TNDT, sounds the main building blocks within the majority of carried out research endeavors. However, very few have investigated and highlighted the importance of combining these three blocks together. For instance, for detection of in-depth defects, the method of “self-referencing” is proposed in [12]. The main drawback with this method is that it analyses only one single image captured at one specific time and does not look at the entire cooling period (image sequence). Therefore, we describe here a novel image analysis approach which exploits a sequence of thermal images and performs a spatiotemporal analysis. Furthermore, in the experiments only the surface temperature of the test specimen are measured, while thermal modelling can provide more detailed information about the temperature distribution within the tested part and around the defected area which could be useful for defect localization and characterization. Hence, this paper also presents a thermal model using the finite element method intended as a base-line model used to simulate different experimental set-ups.

Our purpose is to implement a new image analysis method integrated with thermal modelling and experiments. This paper describes our work so far, and several intertwined steps have been taken; experiment and measurement, image analysis, and thermal modelling and simulation. The acquired measurement data are used in both image analysis and for developing the thermal model.

The paper is organized as follows: In section 2, the experimental setup is described together with carried out measurements. A brief description of the defect detection is given in section 3, while thermal modelling and simulation results are discussed in section 4. Finally, results and conclusions are presented in section 5 and 6.

## 2. Experimental setup

The experiment performed in this study was a pulsed thermography measurement and the temperature distribution over the surface of the test sample was studied during the cooling period. The experiment was carried out using a test sample, a flash lamp as excitation source, an infrared camera, and a data acquisition system in combination with an image processing software package. During the experiment, the flash lamp and the infrared (IR) camera were positioned on the front side of the test sample; in reflection mode, where no defects are visible. The flash lamp was placed at a distance of approximately 250 mm from the test piece, and was oriented perpendicular to it. The camera was positioned behind the flash lamp and was elevated above the level of the flash lamp and the test piece. The experimental setup is shown in figure 1.

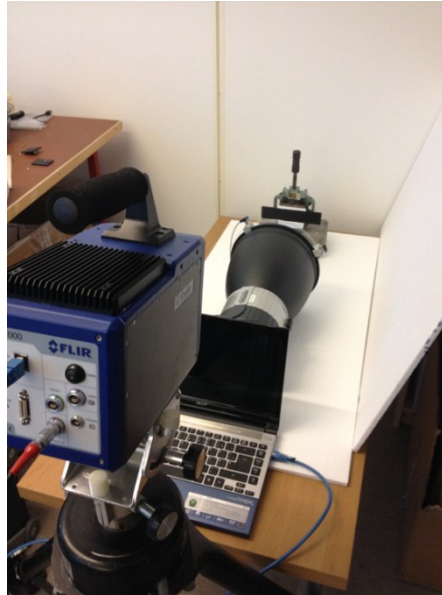


**Fig. 1.** Experimental set-up. The flash lamp was positioned 250 mm in front of the test sample.

The test sample was a 4 mm thick metal plate with small flat-bottom holes of different depths, made of stainless steel (grade 2333/304 SS). Eight flat-bottom holes were drilled in a row from the back side of the plate. All holes were drilled with the same diameter, 2.0 mm, and with different depths ranging from 2.0 mm to 3.5 mm, see figure 2. Parallel to the flat-bottom holes, along the edges of the plate, 16 holes were drilled (through the full thickness of the plate) in order to provide reference positions.

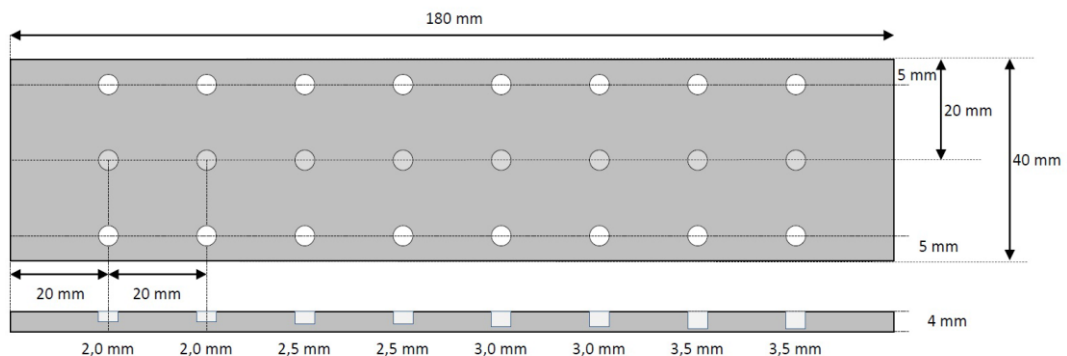


**Fig. 2.** Test sample made of a 4 mm thick steel plate with eight flat-bottom holes, each with 2.0 mm diameter. The holes' depth is ranging from 2.0 mm to 3.5 mm.

Excitation source (flash lamp) was a HENSEL, type of EH Pro-6000, coupled with a HENSEL flash generator type of 6000S. The flash lamp is able to excite energy up to 6 kJ, however, there is no control over excitation time (pulse duration). Metallic surfaces have a high reflectivity in the visual as well as the thermal domain; the high visual reflectivity leads to only a small part of the energy from the flash being absorbed by the test piece, and the low emissivity (high reflectivity) in the thermal domain leads to less robust temperature measurements. To compensate for this, the test piece was coated with black paint, which obviously has a low visual reflectivity (i.e., it is black) and also high emissivity in the thermal domain. Although we did not measure the mid-wave emissivity of this particular paint, black paints commonly have emissivity of around 0.95 in the mid-wave range (see, for example, [14]).

The IR camera used in this test, was a FLIR type of SC7600 with Indium Antimonide (InSb) detector (sensor). The detector operates at mid-wave infrared in the range of 1.5-5.1  $\mu\text{m}$ . The camera has other features such as high temperature sensitivity up to 20 mK, adjustable integration time in nanoseconds, high operating frame-rate up to 870 Hz, and spatial resolution up to 640 x 512 pixels. In the experiment performed in this study, the frame rate was 870 Hz, detector size 160 x 128 pixels, and two calibration curves (covering a temperature range of 20-120  $^{\circ}\text{C}$ ) were used. Then, the chosen frame-rate was shared between the sub-ranges (by the camera); the real frame-rate equals selected frame-rate divided by the number of sub-ranges (calibration curves). Thus, the obtained real frame-rate was 435 Hz (2.3 ms between each frame). In each test, 2000 images were captured during 4.6 s. The ambient temperature was approximately 21  $^{\circ}\text{C}$ .

For data acquisition and basic image processing, the software package AltaIR was used. AltaIR is a software package which is supplied with cooled and science range IR cameras. AltaIR can also be used for image pre-post processing.

### 3. Defect detection

In signal detection or target detection theory, a *test vector*, *test signature* or *probe* is compared to a model of the sought-for target and, possibly, a background model. A special case is *anomaly detection*, where the target is unknown and the test signature is compared to a background model only. This is based on the assumption that targets are rare compared to instances of background, which is a valid assumption in many practical applications.

In this case, it is assumed that most of samples are not covered by cracks and we build a background model of the measured cooling period. The sequence of temperature measurements in a point is regarded as a vector, that is, the vector has one element from each acquired thermal image and the number of vectors equals the number of pixels in the thermal images. The resulting set of vectors is used for building the model. Here a simple low-dimensional linear subspace model is used since this has turned out to give good results; the comparison between each test vector and the background model is done by calculating the squared Euclidean distance to the nearest point in the background subspace. Temporal and spatial median filters for removing noise and artefacts are employed as well. The method is described in more detail in [13]. Example results are shown in figure 3. It is clear that the defect is more clearly pointed out by the proposed compared to the reference method [12].

In order to be able to generalize the results to other materials and defects, a simulation model is needed, which will be treated next.

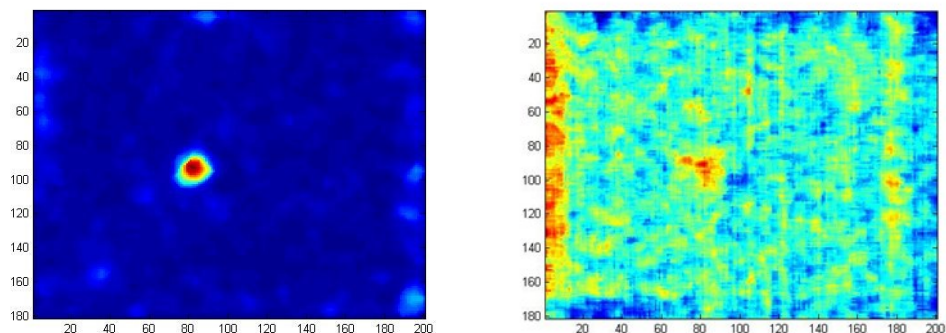


**Fig. 3.** Defect detection using the proposed method (left) and a method from the literature (right). The defect to detect is approximately in the middle of the images. The comparison method is our implementation of the methods by Omar et al. [12].

### 4. Thermal modelling

The geometry of the model consists of a cross section of the test piece including a 3.5 mm deep flat-bottom hole which is illustrated in figure 4. The model is axisymmetric around the axis of the flat-bottom hole. In this 2D axisymmetric cross section, “*r*” represents radius from the centre of the flat-bottom hole, while “*z*” is the depth of the plate.

The mesh was created using an extra-fine element size setting in COMSOL Multiphysics 4.3b. The resulting mesh consists of 1637 unstructured triangular mesh elements with a node distance of 0.12 mm. The model was verified for mesh and time independency, which was achieved for time steps of 0.0002 seconds.

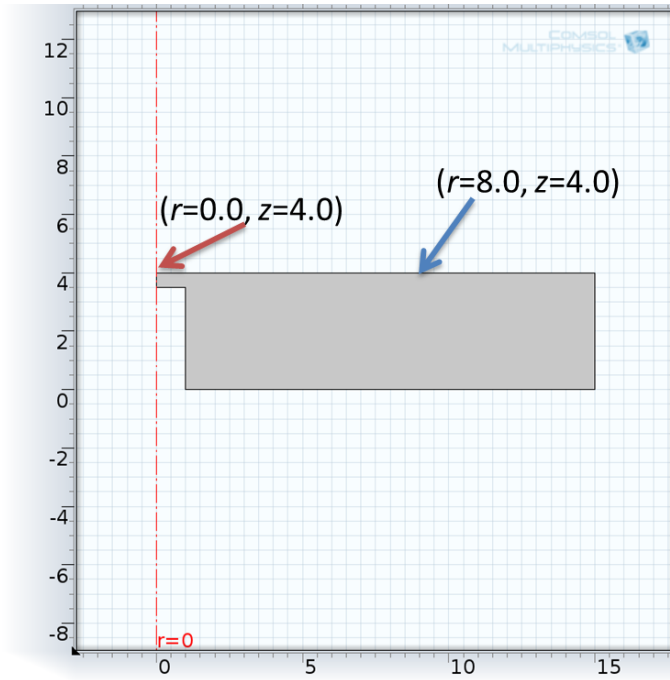


**Fig. 4.** Geometry of the 3.5 mm deep flat-bottom hole.  $z=4.0$  represents the surface of the test piece (equal to the measured surface),  $z=3.5$  is the hole depth, and  $r=0.0$  is the hole's centre-line. Two points on the surface such as  $(r=0.0, z=4.0)$  and  $(r=8.0, z=4.0)$  represent a point right over the defect and the non-defect area, respectively.

The governing equation for 2D axisymmetric transient heat conduction (assuming no heat generation and an isotropic material) can be written as

$$\frac{\partial^2 T}{\partial r^2} + \frac{1}{r} \frac{\partial T}{\partial r} + \frac{\partial^2 T}{\partial z^2} = \frac{\rho C_p}{K} \frac{\partial T}{\partial t}$$

where the transient time is  $t$ ,  $C_p$  denotes the specific heat capacity,  $K$  is the thermal conductivity,  $\rho$  is the density, and  $T$  denotes the temperature. In the model, the initial temperature was set to 21 °C and the boundary conditions are illustrated in figure 5.

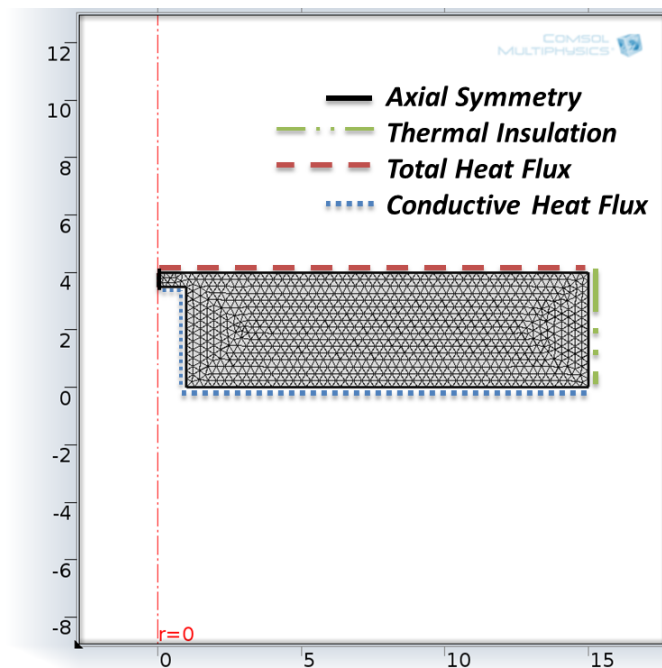


**Fig. 5.** Boundary conditions with extra-fine triangular meshing in the model.

The test sample in this study is made of stainless steel SS 2333. The thermal properties of the material are given in table 1.

**Table 1.** Thermal properties used in the model.

Material	Thermal Conductivity [W/m K]	Specific Heat [J/kg K]	Density [kg/m <sup>3</sup> ]
Metal	15	500	8000
Air	0.025	1005	1.2

**5. Results and discussion**

Two sets of results will be presented and discussed. First, the results which are acquired based on spatiotemporal evolution of surface temperature from experiment and modelling. Then, spatiotemporal evolution of temperature contrast over a defect and non-defect will be given.

An image (captured by the IR camera) of the test piece a few milliseconds after excitation pulse, is presented in figure 6. The areas 1 and 2 correspond to an area just above the flat-bottom hole (defect) and above the defect-free part of the plate, respectively. Since defects can be distinguished from non-defects mainly during the cool-down period, the corresponding temperature-time graphs of areas 1 and 2, for 300 ms (0.03 s) from starting the cool-down period and during the first 10 ms of that period are shown in figure 7 (a) and (b).

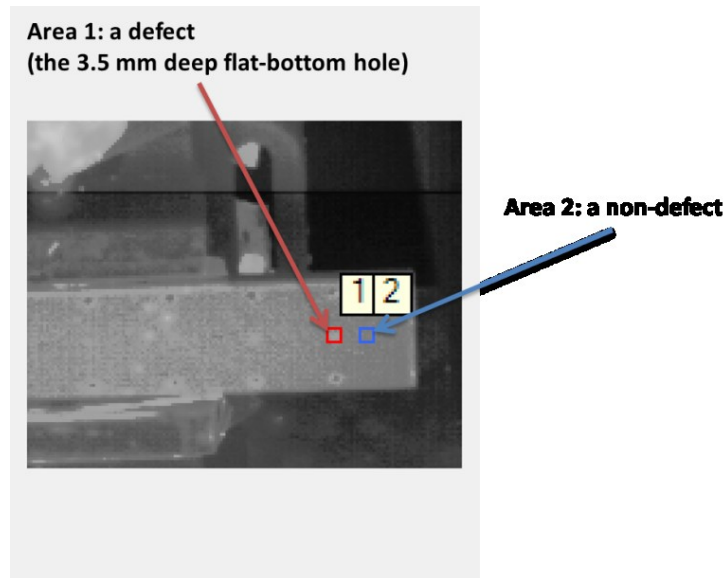


**Fig. 6.** A thermal image acquired after heating excitation by the flash lamp and during the cool-down period.

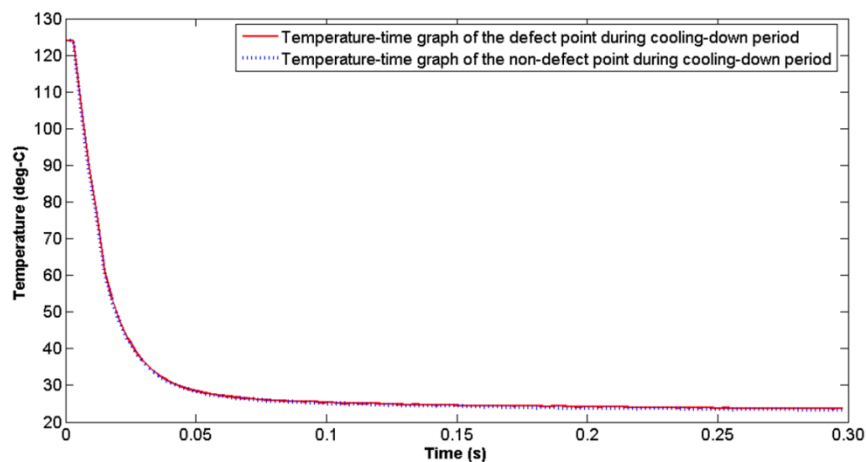


**Fig. 7(a).** Temperature-time graph of the two points, from start of the cool-down period and for 300 ms after. The two points correspond to a defect and a non-defect.

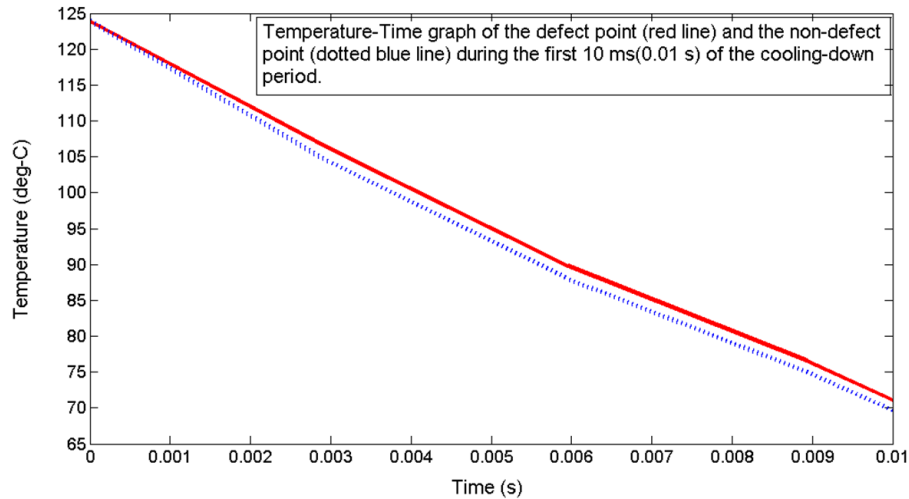


**Fig. 7(b).** Temperature-time graph of the two points (defect and non-defect) during the first 10 ms of the cool-down period. The maximum temperature contrast for approximately 2.0 °C occurs after 4 ms from starting of the cool-down period.

The timing-graph illustrated in figure 7(b) shows that during the cool-down period, the defect point has higher temperature compared to a non-defect point.

The modelling results concerning surface temperature of a defect and a non-defect point is illustrated in figure 8. It can be seen from the numerical results that the point above a defect has slower cooling rate compared to a point above a non-defect. A similar pattern (as in the experimental results) for two surface points corresponding to surface locations right above the defect (radius 0.0 mm) and at the radius 8 mm, can be seen.

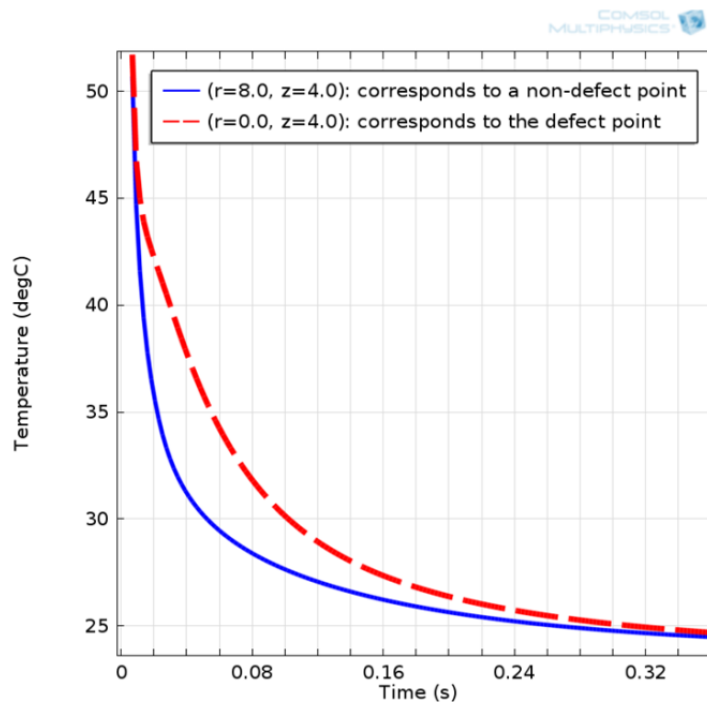


**Fig. 8.** Temperature-time graph corresponds to a defect and a non-defect during the cool-down period. It can be seen that the defect point has higher temperature compared to the non-defect point. In addition, the non-defect point shows a faster cooling rate compared to the defect point. Furthermore, the maximum temperature contrast over the defect and the non-defect point is approximately 7.5 °C which occur at 30 ms after starting the cool-down period.

Finally, temperature contrast over a defect and a non-defect point, resulted from the simulation model and the experiment are illustrated in figure 9.

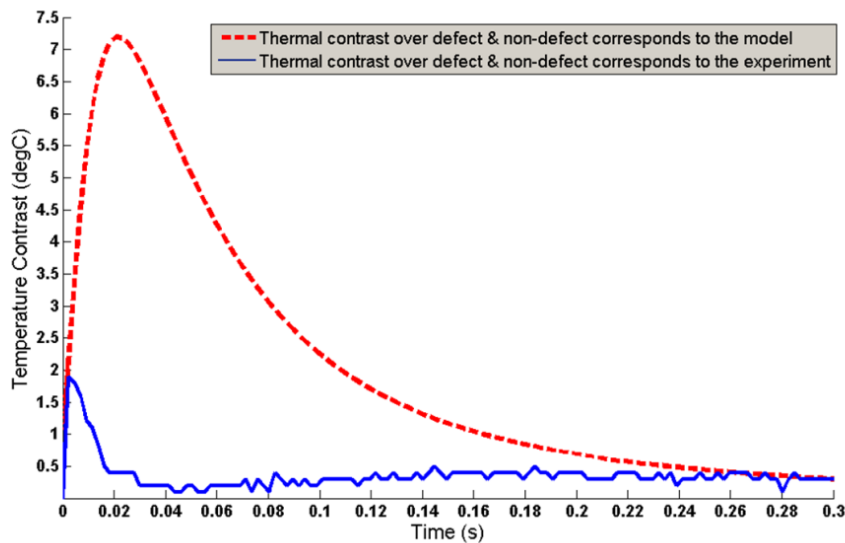


**Fig. 9.** Temperature contrast corresponds to a defect and non-defect on the surface resulted from the model and the experiment.

Comparing the numerical and the experimental results, we can see that the same phenomenon occurs, however, not with the same rate and magnitude. The simulated and the measured temperature contrast, show noticeable differences. In the simulation, the maximum temperature contrast is nearly 7.5 °C which appears at approximately 30 ms, while in the measurement the maximum temperature contrast is approximately 2 °C which occurs at nearly 4 ms.

Several parameters could affect the above mentioned discrepancies. The test piece was coated with an ordinary spray of black paint, of which we did not have any data regarding the thermal properties and thickness of the painted layer. Therefore, the nearly 7.5 °C simulated thermal contrast reveals that the effect of thermally resistive layer should be considered in the model. However, availability of the black paint's data was a challenge.

In general, comparing the experimental and numerical results show considerable differences which could be related to a number of uncertainties regarding performing the tests in real conditions and building the physical model. Uncertainties such as the amount of emitted and absorbed energy, heat pulse duration, pulse shape, and also applying the most suitable boundary conditions by the model which mimics the real conditions.

## 6. Conclusions

We show that the proposed method for defect detection is promising and the achieved results are comparable to the state-of-the-art methods reported in the literature. The data from the thermal modelling shows the same phenomenon as the experimental results; however, still further development of the simulation model is needed in order to have conformity between the simulation and the experimental results. Moreover, results from supplementary measurements with specified thermal properties and thickness of the black paint, could be a support for the simulation model. Therefore, the next step is to improve the model by adding more influencing parameters and mimic the test conditions further, in order to make it a useful simulation tool.

## Acknowledgement

This work was sponsored by the Swedish KK-foundation through the doctoral research school SiCoMaP and by the Swedish Governmental Agency for Innovation Systems (Vinnova) through the project SpotSim. The work on defect detection was sponsored by the Swedish National Space Board through the project TUMD (RyT 200/12).

## REFERENCES

- [1] C. Ibarra-Castanedo, M. Genest, J. M. Piau, S. Guibert, A. Bendada, X. Maldague, "Active infrared thermography techniques for the nondestructive testing of materials", in C. H. Chen (ed.) *Ultrasonic and advanced methods for nondestructive testing and material characterization*, World Scientific Pub Co Inc., 2007.

- [2] C. Ibarra-Castanedo, D. Gonzalez, M. Klein, M. Pilla, S. Vallerand, X. Maldague, "Infrared image processing and data analysis", *Infrared Physics*, 46(1-2):75-83, 2004.
- [3] S. M. Shepard, T. Ahmed, J. R. Lhota, "Experimental consideration in vibro-thermography", *Proc. SPIE* Vol. 5405 (Thermosense XXVI), pp. 332-335, 2004.
- [4] C. Ibarra-Castanedo, A. Bendada, X. Maldague, "Thermographic image processing for NDT", *IV Conferencia Panamericana de END*, Buenos Aires, October 2007.
- [5] T. Soib, M. S. Jadin, S. Kabir, "Thermal imaging for enhancing inspection reliability: detection and characterization", in R. V. Prakash (ed.) *Infrared Thermography*, InTech, 2012. DOI: 10.5772/27558
- [6] N. J. Zalameda, N. Rajic, W. P. Winfree, "A comparison of image processing algorithms for thermal nondestructive evaluation", *Proc. SPIE*, Vol. 5073, 2003.
- [7] S. Marinetti, Y. A. Plotnikov, W. P. Winfree, A. Braggiotti, "Pulse phase thermography for defect detection and characterization", *Proc. SPIE*, Vol. 3586, 1999.
- [8] T. Chen, G. Y. Tin, A. Sophian, P. W. Que, "Feature extraction and selection for defect classification of pulsed eddy current NDT", *NDT&E International*, Vol. 41, pp. 467-476, 2008.
- [9] U. Siemer, "Simulation and evaluation of new thermographic techniques for the deployment in the automotive industry", *Proc. ECNDT*, 2006.
- [10] J. Vrana, M. Goldammer, J. Baumann, M. Rothenfusser, W. Arnold, "Mechanisms and models for crack detection with induction thermography", *Review of quantitative non-destructive evaluation*, Vol. 27, 2008.
- [11] M. Louaayou, N. Nait-Said, F. T. Louai, "2D finite element method study of the stimulation induction heating in synchronic thermography NDT", *NDT&E International* Vol. 41, pp. 575-581, 2008.
- [12] M. Omar, M. I. Hassan, K. Saito, and R. Alloo. "IR self-referencing thermography for detection of in-depth defects", *Infrared Physics and Technology*, Vol. 46, pp. 283-289, 2005.
- [13] K. Höglund, *Non-destructive testing using thermographic image processing*, MSc thesis no. LiTH-ISY-EX-13/4655-SE, Linköping University, 2013.
- [14] A. M. Baldrige, S. J. Hook, C. I. Grove and G. Rivera, "The ASTER Spectral Library Version 2.0", *Remote Sensing of Environment*, vol 113, pp. 711-715, 2009. <http://speclib.jpl.nasa.gov>